

## THERMAL EVOLUTION AND STRUCTURE MODELS OF THE TRANSITING SUPER-EARTH GJ 1214B

N. NETTELMANN<sup>1,2</sup>, J. J. FORTNEY<sup>1,3</sup>, U. KRAMM<sup>2</sup> AND R. REDMER<sup>2</sup>

*Accepted to ApJ, 03/2011*

### ABSTRACT

The planet GJ 1214b is the second known super-Earth with a measured mass and radius. Orbiting a quiet M-star, it receives considerably less mass-loss driving X-ray and UV radiation than CoRoT-7b, so that the interior may be quite dissimilar in composition, including the possibility of a large fraction of water. We model the interior of GJ 1214b assuming a two-layer (envelope+rock core) structure where the envelope material is either H/He, pure water, or a mixture of H/He and H<sub>2</sub>O. Within this framework we perform models of the thermal evolution and contraction of the planet. We discuss possible compositions that are consistent with  $M_p = 6.55 M_\oplus$ ,  $R_p = 2.678 R_\oplus$ , an age  $\tau = 3 - 10$  Gyr, and the irradiation level of the atmosphere. These conditions require that if water exists in the interior, it must remain in a fluid state, with important consequences for magnetic field generation. These conditions also require the atmosphere to have a deep isothermal region extending down to 80–800 bar, depending on composition. Our results bolster the suggestion of a metal-enriched H/He atmosphere for the planet, as we find water-world models that lack an H/He atmosphere to require an implausibly large water-to-rock ratio of more than 6:1. We instead favor a H/He/H<sub>2</sub>O envelope with high water mass fraction ( $\sim 0.5$ – $0.85$ ), similar to recent models of the deep envelope of Uranus and Neptune. Even with these high water mass fractions in the H/He envelope, generally the bulk composition of the planet can have subsolar water:rock ratios. Dry, water-enriched, and pure water envelope models differ to an observationally significant level in their tidal Love numbers  $k_2$  of respectively  $\sim 0.018$ ,  $\sim 0.15$ , and  $\sim 0.7$ .

*Subject headings:* planets and satellites: general — planets and satellites: individual(GJ 1214b)

### 1. INTRODUCTION

Among the nearly 500 detected planet candidates, and in particular among the  $\sim 80$  planets for which both the mass and radius have been determined, our Earth is the only planet that is known to harbor liquid water oceans on a solid surface crust. These conditions have proven favorable for the development of life forms. With the discovery of CoRoT-7b ( $M_p = 4.8 \pm 0.8 M_\oplus$ ; Léger et al. 2009) and GJ 1214b ( $M_p = 6.55 \pm 0.98 M_\oplus$ ; Charbonneau et al. 2009), the search for other habitable worlds has just recently passed the milestone of discovering transiting extrasolar planets in the 2-10  $M_\oplus$  super-Earth mass regime.

Higher-mass planets such as Uranus ( $M_p = 14.5 M_\oplus$ ) are predicted by interior models to retain a H/He-rich atmosphere (Hubbard et al. 1995) whose size may vary depending on  $M_p$ ,  $R_p$  and temperature. Pressures at the bottom of this envelope are high, and may reach 1 to 1000 kbar if the planet is of Neptune-size (Nettelmann et al. 2010) or even several Mbar if of Saturn-size (Guillot 1999) before a presumably solid core is reached. Lower-mass objects on the other hand such as Mars or Ganymede have been observed not to retain a thick enough atmosphere that could prevent the planet's surface from cooling below the freezing point of water.

CoRoT-7b –orbiting a Sun-like star at short orbital distance  $a_p = 0.017$  AU– falls into the intermediate super-Earth mass regime; the stellar extreme ultraviolet (EUV) flux it receives is so strong that its current

atmosphere is either a tiny remnant of an initially massive gaseous envelope, or hot evaporating core material at an equilibrium temperature  $T_{\text{eq}} = 1800 - 2600$  K (Valencia et al. 2010; Jackson et al. 2010). In contrast, GJ1214b ( $a_p = 0.0144$  AU) orbits an M star of  $\sim 3 \times 10^{-3}$  smaller luminosity (Charbonneau et al. 2009) translating into a planet-average  $T_{\text{eq}} \leq 555$  K, only a factor of two higher than that of Earth. Hence the discovery of GJ1214b manifests an important step toward a detection of an extrasolar ocean planet.

Rogers & Seager (2010) investigated the response of interior models to the uncertainties in  $M_p$ ,  $R_p$ , and intrinsic temperature  $T_{\text{int}}$  and showed that GJ1214b might have a  $(10^{-4} - 0.068) \times M_p$  thick H/He atmosphere, or else an outgassed H atmosphere, or a water envelope atop a silicate-iron core with an ice:rock (I:R) ratio of 0.06 to  $\infty$ .

In this paper we adopt the fiducial  $\{M_p, R_p\}$  values and investigate how the unknown temperatures of the deep interior can be constrained by thermal evolution calculations. Our models are two-layer models with one homogeneous envelope overlying a rock core. We take into account mass loss during evolution and explore how that affects the possible mass of an outer H/He layer (§ 3.1). In § 3.2 we consider pure water atmospheres and ask whether condensation or even solidification of water could then have occurred within 10 billion years of cooling. In line with recent transmission spectrum measurements that indicate 70% or more water by mass in the atmosphere (Bean et al. 2010), we vary in § 3.3 the envelope water mass fraction between 50 and 100% and suggest plausible models with about 0.2×solar I:R ratio. In § 4 we discuss our model assumptions and propose to

<sup>1</sup> Department of Astronomy and Astrophysics, University of California, Santa Cruz, CA 95064

<sup>2</sup> Institut für Physik, Universität Rostock, D-18051 Rostock

<sup>3</sup> Alfred P. Sloan Research Fellow

discriminate between our three classes of models (dry, water, water-rich envelope) by observationally determining the Love number  $k_2$  and the mean molecular weight of the atmosphere. Our method of modeling this planet is explained in § 2, where we describe the irradiated atmosphere grid (§ 2.1), applied equations of state (§ 2.2), mass loss (§ 2.3), and the calculation of structure and evolution (§ 2.4).

## 2. METHODS

In this section we describe the four components that our interior models rely on: the model atmosphere grid, the equations of state used, structure assumptions, and the thermal evolution to the present state. The evolutionary models have some similarities to what has previously been applied to hot Neptunes and hot Jupiters (e.g. Fortney et al. 2007; Baraffe et al. 2008), but with additional complications due to radiogenic heating. As the planet’s interior cools, the external radiative zone grows deeper (Guillot et al. 2006), reaching a depth of up to several hundreds of bars. The transition pressure of the atmosphere from radiative to adiabatic, at the current time,  $P_{ad}(t_0)$ , is a quantity we aim to constrain with our evolution model. We also perform explorations of the planet’s structure as a function of  $P_{ad}(t_0)$ , to investigate the full range of hotter, higher entropy interiors (lower  $P_{ad}(t_0)$ ) and cooler, lower entropy interiors (higher  $P_{ad}(t_0)$ ) that may be possible today.

### 2.1. The model atmosphere

Under the assumption the deep envelope layers convect efficiently, it is the radiative atmosphere atop the convective region that serves as the bottleneck for interior cooling, just as in Neptune, Uranus, and giant planets generally (e.g., Hubbard 1977). Observations of GJ1214b’s atmosphere are consistent with a water-dominated composition as well as with a H/He atmosphere with clouds or hazes (Bean et al. 2010). Given our current ignorance of the composition of the atmosphere, we consider the two likely end-member cases, either a H/He-dominated atmosphere, or a pure steam atmosphere, and find that the opacity is dominated by water vapor in either case (Miller-Ricci & Fortney 2010). For planetary structure, we assume chemical equilibrium in the atmosphere, thereby ignoring possible alterations of the T-P profile through photoionization.

For planetary evolution, a grid of model atmospheres is generally used as the upper boundary condition, see, for instance, Fortney et al. (2007). These grids relate the specific entropy ( $s$ ) of the convective interior, surface gravity ( $g$ ) of the planet, and the intrinsic effective temperature ( $T_{\text{int}}$ ) from the interior. We have computed such a grid from  $T_{\text{int}} = 175$  K down to 30 K, with the correct limiting behavior down to 0 K (an exhausted interior) across surface gravities from 100 to 1500  $\text{cm s}^{-2}$ . The grid is computed at  $50\times$  solar metallicity, under the assumption of complete redistribution of absorbed stellar flux (meaning  $f=1/4$ , see Fortney et al. 2007; Miller-Ricci & Fortney 2010), and no clouds. Similar models, which describe the technique in more detail, are found in Fortney et al. (2007). The opacity database is described in Freedman et al. (2008). We note that this very high metallicity is realistic given that Nep-

tune and Uranus are 30-60 times solar in carbon (see Guillot & Gautier (2009), for a review).

We use this grid for all evolution calculations of our models, whether they possess thin H/He - atmospheres or pure steam atmospheres. This is certainly a broad brush treatment for a wide range of possible atmospheres, but given our current ignorance regarding the planet’s atmosphere, we feel our treatment is justified. The importance and utility of the coupled model atmosphere/interior cooling calculation is that it allows us to estimate  $T_{\text{int}}$  and  $P_{ad}$  as a function of time. For instance, in the recent work of Rogers & Seager (2010), the value of  $T_{\text{int}}$  was not calculated, but was extrapolated from evolutionary models of Baraffe et al. (2008), for higher mass objects. Generally, we find a 15 K lower  $T_{\text{int}}$ , meaning a colder interior, than Rogers & Seager (2010) used. While  $T_{\text{int}}$  may change from 175 down to 30 K during evolution, we find that the effective temperature  $T_{\text{eff}}$  remains nearly constant within 562 to 557 K, which is close to the zero-albedo, planet-average equilibrium temperature of 555 K.

### 2.2. Equations of state

Metal-rich<sup>4</sup> planets such as super-Earths are generally suspected to harbour a variety of materials. We aim to represent this variety in a simplified manner by confining silicates and iron into a ‘rocky’ core, and H, He, and water to an envelope. For core material we use the  $P - \rho$  relation for rocks by Hubbard & Marley (1989) which describes an adiabatic mixture around  $10^4$  K of 38%  $\text{SiO}_2$ , 25%  $\text{MgO}$ , 25%  $\text{FeS}$ , and 12%  $\text{FeO}$ . Such kind of rocks’ mass fraction of Si, Mg, and Fe is, respectively, about 0.5, 0.62, and 1.05 times that of the bulk Earth (McDonough & Sun 1995). For H/He envelopes we use the interpolated hydrogen and helium EOS developed by Saumon et al. (1995). For water we use  $\text{H}_2\text{O}$ -REOS, which was applied to Jupiter (Nettelmann et al. 2008), Uranus and Neptune (Fortney et al. 2010b) and in a slightly modified version to CoRoT-7b (Valencia et al. 2010). This water EOS comprises various water EOS appropriate for different pressure-temperature regimes. It includes the melting curve and phase Ice I (Feistel & Wager 2006), the saturation curve and liquid water (Wagner & Pruß 2002), vapor and supercritical molecular water (SESAME 7150, Lyon & Johnson 1992), and for  $T \geq 1000$  K and  $\rho \geq 2$   $\text{g cm}^{-3}$  supercritical molecular water, ionic water, superionic water, plasma, ice XII, and ice X based on FT-DFT-MD simulations (French et al. 2009). At pressures below 0.1 GPa, and/or temperatures below 1000 K,  $\text{H}_2\text{O}$ -REOS relies on Sesame EOS 7150 (Lyon & Johnson 1992). For mixtures of hydrogen, helium, and water we use H-REOS for hydrogen (Nettelmann et al. 2008),  $\text{H}_2\text{O}$ -REOS for water, and an improved version (Kerley 2004) of the helium Sesame EOS 5761 (Lyon & Johnson 1992). Other materials are not considered here<sup>5</sup>.

<sup>4</sup> The label *metals* comprises all elements heavier than H and He.

<sup>5</sup> We do not consider the lighter and more volatile ices  $\text{CH}_4$  and  $\text{NH}_3$ . We performed simple tests by perturbing warm  $\text{H}_2\text{O}$ -REOS adiabats with the zero-temperature  $P - \rho$  relations for  $\text{CH}_4$  and  $\text{NH}_3$  by Zharkov & Trubitsyn (1978). In a solar C:N:O proportion, this reduces the density by  $\sim 0.5$   $\text{g cm}^{-3}$  if  $P > 20$  GPa, but enhances the density for smaller pressures, due to neglect of

### 2.3. Mass loss

Mass escape caused by stellar energy input is known to occur from the highly irradiated atmosphere of the hot Jupiter HD 209458b (Vidal-Madjar et al. 2003; Yelle 2004; Erkaev et al. 2007; Murray-Clay et al. 2009), and shown to have a significant impact on the current composition of super-Earth CoRoT-7b (Valencia et al. 2010; Jackson et al. 2010). While the sun-like star CoRoT-7 irradiates the planet with a present X-ray and ultraviolet energy flux (XUV)  $F_{\text{XUV}} = 5 \times 10^5 \text{ erg cm}^{-2} \text{ s}^{-1}$  (Valencia et al. 2010), GJ 1214 is supposed to be an inactive M star (Charbonneau et al. 2009). Assuming it obeys the empirical relation for the surface energy flux of M stars,  $F_{\star, \text{XUV}}/F_{\star, \text{bol}} = (1 - 100) \times 10^{-5}$  (Scalo et al. 2007), then with  $L_{\star} = 0.0033L_{\odot}$ ,  $R_{\star} = 0.211R_{\odot}$ , the energy flux  $F_{\text{XUV}} = F_{\star, \text{XUV}}(R_p^2/4a_p^2)$  received by GJ 1214b is only  $(0.8 - 80) \text{ erg cm}^{-2} \text{ s}^{-1}$ , i.e.  $(0.16 - 16) \times 10^{-4}$  that of CoRoT-7b, at the current time. We then expect XUV irradiation to have a comparatively lesser, but still important, influence on the atmospheric mass through time.

We use the energy limited escape model of Erkaev et al. (2007) to investigate the mass-loss history of the planet. With a heat absorption efficiency  $\varepsilon = 0.4$ , and a correction factor  $K_{\text{tide}} = 0.95$  accounting for the height decrease of the Roche-lobe boundary through tidal effects (Erkaev et al. 2007), the energy-limited mass escape rate  $\dot{M}_{\text{esc}} = (\varepsilon F_{\text{XUV}} R_p^3) (G M_p K_{\text{tide}})^{-1}$  (following Valencia et al. 2010) is  $(0.012 - 2.8) \times 10^8 \text{ g s}^{-1}$ . This is  $\approx (0.02 - 6) \times 10^{-3}$  the mass loss of present (rocky) CoRoT-7b, with a value of  $(1 - 100) \times 1.84 \times 10^6 \text{ g s}^{-1}$ , for the fiducial GJ 1214b values  $M_p = 6.55 M_{\oplus}$  and  $R_p = 2.678R_{\oplus}$ . Correcting  $\dot{M}_{\text{esc}} \sim r_1^2 R_p$  for the altitude  $r_1 > R_p$  where the XUV flux is absorbed (Lammer et al. 2003), the actual value can further rise by a factor of 10. Within 1 Gyr, this mass loss accumulates to  $(1 - 100) \times 10^{-4} M_{\oplus}$ . For a low-mass atmosphere of only about 1% of GJ 1214b’s total mass (which is quite possible for a small mean molecular weight atmosphere: see § 3.1), the fraction of the atmosphere lost during the 3 to 10 Gyr lifetime of this planet can be large enough to influence its cooling behavior. In particular, according to the estimates above and assuming constant mass loss over time, the initial atmosphere can have been larger by  $(1 - 100) \times (0.5 - 1.5)\%$ . We therefore must include mass loss in our evolution calculations of H/He envelope models, as described below.

### 2.4. Interior structure and evolution modeling

*Three classes.* We consider three classes of hydrostatic two-layer interior models of present GJ 1214b assuming a homogeneous envelope above a rocky core. The three classes differ in the materials constituting the envelope. Class I models have a H/He envelope with solar He mass fraction  $Y = M_{\text{He}}/(M_{\text{H}} + M_{\text{He}}) = 0.27$ . Class II models have a pure water envelope (“water worlds”), and class III models a H/He/H<sub>2</sub>O envelope with variable water mass fraction  $Z_1$ , and also  $Y = 0.27$ . The rock core mass of present GJ 1214b

finite temperature effects which are important for supercritical ices. Since these EOS are not of comparable quality to those used for all other components, we do not include them here.

models is found by the condition to match the radius  $R_p = 2.678R_{\oplus}$  (recently confirmed through both optical and infrared photometry (Sada et al. 2010)) for a given planet mass  $M_p = 6.55M_{\oplus}$  and surface thermal boundary condition. We do not consider different possible  $R_p - M_p$  pairs within the observational error bars  $\sigma_{M_p} = \pm 1.0M_{\oplus}$  and  $\sigma_{R_p} = \pm 0.13R_{\oplus}$  as such work has already been presented by Rogers & Seager (2010). For the thermal structure of the atmosphere we apply the solar composition model atmosphere between 20 mbar and 10 bar to model classes I and III, and to model class II the water model atmosphere between 20 mbar and 1 bar from Miller-Ricci & Fortney (2010). At higher pressure in the radiative atmosphere, we assume an isothermal temperature—a reasonable assumption (Miller-Ricci & Fortney 2010) and given our general understanding of highly irradiated atmospheres.

*Calculating the structure.* We choose 20 mbar as the low-pressure boundary of our models. This is a choice of convenience, since our water EOS ends at this pressure, but it is also realistic. The wide-band optical transit radius for the planet is at  $\sim 10$  mbar (E. Miller-Ricci, personal communication). This is consistent with the cloud-free atmosphere calculations of Fortney et al. (2003) for HD 209458b, as well.

The high-pressure boundaries of the model atmospheres of respectively 1 and 10 bar are chosen within the isothermal part of the atmosphere, before it transitions to the adiabatic interior at some pressure  $P_{ad}$ . For present time ( $t_0$ ) structure models, we consider the transition pressure  $P_{ad}(t_0)$  a variable parameter and investigate the response of the core mass and the cooling time on the choice of  $P_{ad}(t_0)$ .

Since the model atmospheres predict almost constant equilibrium abundances of H, He, and H<sub>2</sub>O, we derive the mass density  $\rho(P, T(P))$  in the atmosphere  $T(P)$  from an EOS table for constant composition. Given  $M_p$ ,  $R_p$ , and the  $P - \rho$  relations according to the EOS  $\rho(P, T(P))$  in the atmosphere, and constant  $s(P, T, \rho(P, T))$  in the adiabatic interior, we obtain internal profiles  $m(r)$ ,  $T(r)$ , and  $P(r)$  by integrating the equation of hydrostatic equilibrium  $dP/dr = -Gm\rho/r^2$  from the surface toward the center. Mass conservation  $M_p = \int_0^{R_p} dr 4\pi r^2 \rho(r)$  is ensured by the proper choice of the rock core mass  $M_{\text{core}}$ .

*The rock core assumption.* We assume the rocky core to be appropriately described by an EOS of *homogeneous, adiabatic* ‘rocks’ at all times (compare Rogers and Seager 2010: differentiation into an iron core and a silicate layer of Mg<sub>0.1</sub>Fe<sub>0.1</sub>SiO<sub>3</sub> at uniform temperature). Differentiation will have occurred when temperatures in the primitive rock core rose above the melting temperature of iron during formation, and will have affected the thermal evolution. In the Earth, solidification of the inner iron core still causes a buoyancy of light elements driving convection of the outer iron core, and supports—together with gravitational energy release from core shrinking—subsolidus convection of the silicate mantle. If the melting line of iron rises steeply with temperature as indicated by ab initio data (see Valencia et al. 2010, for an overview), also the central part of a several earth mass core of GJ 1214b might transition from liquid to solid iron due to high pressure up to  $\sim 15$  Mbar, supporting

the assumption of an adiabatic interior.

Due to the poorly constrained iron mass fraction of GJ 1214b and uncertainties in the iron melting line, the deep interior could potentially be fully liquid or solid and isothermal. Since the equations of state of rocky materials at high pressure above few Mbar are not well known and the effect of temperature on the  $P - \rho$  relation is negligible (Seager et al. 2007), we believe the  $P - \rho$  relation of the rock-EOS used is appropriate for our purpose of determining the core mass and its contribution to the cooling time. We denote by  $T_{core}$  the temperature at the core-mantle boundary and assume its time derivative  $T_{core}/dt$  to be representative for the whole core.

*Calculating the evolution.* Choosing  $P_{ad}(t_0)$  for class I and II models, and  $P_{ad}(t_0)$  and  $Z_1$  for class III models uniquely defines the core mass of resulting interior models. A selection of six such present time interior models is shown in Table 1. For class I and II models, we calculate the cooling curve by first generating  $\sim 50$  profiles with decreasing transition pressures  $P_{ad}(t_0) \geq P_{ad} > 20$  mbar values, thereby increasingly warmer interiors. For each of these intermediate profiles, core mass and composition are conserved. As the interior becomes warmer with decreasing  $P_{ad}$ , the planet radius  $R_p$  rises. In order to obtain the cooling curve  $R_p(t)$ , we integrate the energy balance equation

$$L_{\text{eff}} - L_{\text{eq}} = -\frac{dE_{\text{int}}}{dt} \quad (1)$$

backward in time, starting with the present time structure models. In Eq.(1),  $L_{\text{eff}} = 4\pi R_p^2 \sigma T_{\text{eff}}^4$  is the net luminosity the planet radiates into space, and  $L_{\text{eq}} = 4\pi R_p^2 \sigma T_{\text{eq}}^4$  is the stellar energy absorbed. The difference  $L_{\text{eff}} - L_{\text{eq}} \sim T_{\text{int}}^4$  is provided by our atmosphere grid  $T_{\text{int}}(g, s)$ , see § 2.1, and sets the intrinsic luminosity the planet can radiate away from the interior through its atmosphere at a given gravity and internal entropy. Given  $T_{\text{int}}$ , we can then derive the time interval  $dt$  it needs to lose the intrinsic energy  $dE_{\text{int}}$ ,

$$\frac{dE_{\text{int}}}{dt} = \int_{M_{\text{core}}}^{M_p} dm \frac{T ds}{dt} + c_v M_{\text{core}} \frac{dT_{\text{core}}}{dt} - L_{\text{radio}}. \quad (2)$$

Expression (2) accounts for the heat loss  $\delta q = T(m)ds$  of each envelope mass shell  $dm$ , the heat loss of the core due to cooling, and the energy gain  $L_{\text{radio}}$  of rocky core material due to decay of radioactive elements (see below).

Experimental data for the specific heat  $c_v$  of warm, compressed rocks at  $P > 2$  Mbar are not available. Ab initio calculations for iron at a few Mbar and several thousand K (Earth's core conditions) predict  $c_v \approx 0.5 \text{ J K}^{-1} \text{ g}^{-1}$  (Alfè et al. 2001), while  $c_v = 1.0 \text{ J K}^{-1} \text{ g}^{-1}$  was formerly applied by Guillot et al. (1995) to the core of Jupiter and by Valencia et al. (2010) to the silicate-iron interior of CoRoT-7b. We aim to bracket the uncertainty in  $c_v$  by choosing  $c_v = 0.5 - 1.0 \text{ J K}^{-1} \text{ g}^{-1}$ . For given  $T_{\text{int}}$ , the time interval required to lose  $E_{\text{int}}$  rises with  $c_v$ .

*Radiogenic heat.* As we will see, our class I and III planet models have large rocky cores. Modeling the radiogenic heat from the rocky portion of the interior is important to accurately calculate the thermal evolution. For  $L_{\text{radio}}$  we consider the isotopes  $^{238}\text{U}$ ,  $^{235}\text{U}$ ,  $^{232}\text{Th}$ , and

$^{40}\text{K}$ . We adopt isotopic abundances and element abundances of meteorites for the elements U, Th, K, and Si<sup>6</sup> as given in Anders & Grevesse (1989). With respective half-life times in Gyrs of 4.468, 0.704, 14.05, and 1.27, and respective decay energies in MeV of 4.27, 4.679, 4.083, and 1.33<sup>7</sup>, we find a radioactive energy release for  $1M_{\oplus}$  of meteoric material on Earth today of  $2.3 \times 10^{13} \text{ J s}^{-1}/1M_{\oplus}$  ( $=: L_{\text{radio,meteor}}(t_0)$ ) and 4.56 Gyr ago of  $2.7 \times 10^{14} \text{ J s}^{-1}/1M_{\oplus}$  ( $=: L_{\text{radio,meteor}}(0)$ ). The dominant contribution during this time interval is mostly due to  $\beta^-$  decay of  $^{40}\text{K}$  into  $^{40}\text{Ca}$ . Extension of the radioactive decay law to 10 Gyr ago would increase  $L_{\text{radio}}$  to  $20 \times L_{\text{radio,meteor}}(0)$ , an unrealistically high value for rock material in the young universe. Of course, for small core masses ( $0.1M_p$ ), cooling of the core does not significantly affect the model's cooling time, but for large core mass models it does, and in particular the choice of the initial value  $L_{\text{radio}}(0)$  matters. Therefore, we define a cosmological luminosity  $L_{\text{cosmo}} := L_{\text{radio,meteor}}(0)$  that we require each cooling model of GJ 1214b to start with, within 10%. Models with long cooling times (10 Gyr) will then have  $L_{\text{radio}}(t_0) \approx 0.1 \times L_{\text{radio,meteor}}(t_0)$ , and models with short cooling times (3 Gyr) will have  $L_{\text{radio}}(t_0) \approx 2 \times L_{\text{radio,meteor}}(t_0)$ . By this choice of  $L_{\text{cosmo}}$  we avoid extremely high or low initial values.

*Evolution with mass loss.* For a given planet radius, low mean molecular weight atmospheres or envelopes are also of low mass, and hence such envelopes may lose a larger relative mass fraction than large mean molecular weight atmospheres. We take into account mass loss only for the H/He envelope models, e.g. models Ia,b in Table 1. For each neighbored pair of interior profiles as given by  $P_{ad}$ , we calculate the mass  $dM$  lost during a time interval  $dt$  self-consistently using a Newton-Raphson scheme to find the root of the function  $f(dt(dM)) = dM - \dot{M}_{\text{esc}} dt(dM) = 0$ .

*Other contributions.* We did not include the effect of tidal heating due to tides raised on the planet by the star. This additional amount of energy would tend to delay the cooling time, in particular in the past when the eccentricity  $e$ , and hence the tidal heating  $dE/dt \sim (e^2/a_p^6)$  (to second order in  $e$ , e.g.; Batygin et al. 2009b), was larger than today. On the other hand, inclusion of tidal migration  $\dot{a}_p$  of the planet would have reduced the amount of stellar irradiation received at early times (Miller et al. 2009). A proper treatment of both effects is beyond the scope of this paper since the orbital eccentricity is not well-constrained (Charbonneau et al. 2009). Instead, we make the standard assumption that the formation of GJ 1214b yielded an initial heat of accretion that was not released before the planet arrived at its current location.

The cooling time of our thermal evolution models is the time between the present state and the time when the derivative  $dT_{\text{eff}}/dt$  approaches  $-\infty$ , which corresponds to a hot start that is insensitive to the initial conditions. While such a treatment of young planets is common (e.g.; Baraffe et al. 2003), it actually ignores the

<sup>6</sup> The Si mass abundance of meteorites (10.65%) is unequal that of the rock EOS (16.8%).

<sup>7</sup> These values are in part an average over the surprisingly wide spread of literature values, see e.g. <http://ie.lbl.gov/education/>, and in part over decay chains ( $^{40}\text{K}$ )

**Table 1**  
GJ 1214b structure model input and output data

Label	$M_{core}$ ( $M_{\oplus}$ )	$P_{ad}(t_0)$ (bar)	$Z_1$	envelope material	$\dot{M}$ ( $10^7$ g/s)	$k_2$	$T_{int}$ (K)	age (Gyr)
Ia	6.464	300	0	H/He	1.84	0.0183	42.7	3.1
Ib	6.434	800	0	H/He	1.84	0.0170	31.8	7.2
IIa	0.873	80	1	water	-	0.5769	51.9	3.05 - 3.16
IIb	0.203	300	1	water	-	0.737	37.6	9.23 - 9.26
IIIa	4.432	120	0.85	H/He/water	-	0.14336	48.4	2.92 - 3.22
IIIb	4.016	400	0.85	H/He/water	-	0.186	35.6	9.21 - 10.10

**Note.** — These structure models have  $R_p = 2.678R_{\oplus}$  and  $M_p = 6.55M_{\oplus}$ .

process of planet formation which has been shown to alter the luminosity during the first tens of millions of years (Fortney et al. 2005). This is important for mass determinations from cooling tracks, whereas in our case it just might induce an error of  $\sim 10$  Myrs to the calculated cooling time.

*Love number  $k_2$ .* We follow the call by Ragozzine & Wolf (2009) to tabulate the tidal Love Number  $k_2$  values of representative models. This quantity is a planetary property which solely depends on the internal density distribution. If known,  $k_2$  imposes an additional constraint on interior structure models. Physically,  $k_2$  quantifies the quadrupolic gravity field deformation at the surface in response to an external perturbing body of mass  $M$ , which can be the parent star, another planet, or a satellite.  $M$  causes a tide-raising potential  $W(r) = \sum_{n=2} W_n = (GM/a) \sum_{n=2} (r/a)^n P_n(\cos \psi)$ , where  $a$  is the distance between the centers of mass (planet and body),  $r$  is the radial coordinate of the point under consideration inside the planet,  $\psi$  is the angle between the planetary mass element at  $r$  and the center of mass of  $M$  at  $a$ , and  $P_n$  are Legendre-Polynomials. Each external potential's pole moment  $W_n(r)$  induces a change  $V_n(r)$  in the corresponding degree of the planet's potential, where  $V_n(R_p) = k_n W_n(R_p)$  defines the Love numbers. For the calculation of  $k_2$  we follow the approach described in Zharkov & Trubitsyn (1978).

To first order in the expansion of the planet's potential,  $k_2$  is proportional to the gravitational moment  $J_2$  (see e.g. Hubbard 1984, § 4). That is why measuring  $k_2$  will provide a constraint for extrasolar planets that is equivalent to  $J_2$  for the solar system planets. In particular,  $k_2$  is known to be a measure of the central condensation of an object, which can be parameterized by the core mass within a two-layer model approach. However, as for  $J_2$ , the inverse problem—the deduction of the internal density distribution of the planet from  $k_2$ , is non-unique.

We stress that the Love number  $k_2$  is a *potentially observable parameter* if the planet's eccentricity is non-zero. It can be obtained with the help of transit light curves that contain information about the tidally induced apsidal precession of close-in planets (Ragozzine & Wolf 2009), or for specific two-planet systems can also be derived from measuring the orbital parameters (Batygin et al. 2009b), given that the planets are in apsidal alignment and on co-planar orbits (Mardling 2010).

### 3. RESULTS

The framework of the three structure classes I-III is used to investigate the possible set of models with respect

to core mass, internal pressures and temperatures, water to rock ratio, and the H/He mass fraction.

#### 3.1. GJ 1214b with a H/He atmosphere and a rock core

For our H/He envelope+rock core models we find a narrow core mass fraction range of 0.975–0.995 for a wide pressure range  $50 \leq P_{ad}(t_0) \leq 4000$  bar (Fig. 1a). Despite its low mass fraction, the H/He envelope extends over  $0.37 R_p$  (Fig. 1b) independent of the envelope mass. This is because of its high temperature, which increases from 1030 K at  $P_{ad}(t_0)$  to 2400–4200 K at  $\sim 35$ –90 kbar at the envelope-core boundary. At these conditions, hydrogen is molecular throughout the envelope according to the SCvH-i EOS.

Not all of the models shown in Fig. 1a,b are consistent with an age  $\tau_* = 3$  to 10 Gyr of the star GJ 1214. If  $P_{ad}(t_0)$  decreases (increases), internal entropy rises (falls) and the planet will need less (more) time to cool down to this state. This behavior is illustrated by the cooling curves in Fig. 1c, according to which an age of 3 Gyr requires  $P_{ad}(t_0) \geq 300$  bar; and a much longer cooling time of 7.2 Gyr is obtained for  $P_{ad}(t_0) = 800$  bar, whereas  $P_{ad}(t_0) = 100$  bar would give a cooling time below 1 Gyr. With a mass loss rate according to  $F_{XUV}/F_{bol} = 10^{-5}$  as assumed for the cooling curves in Fig. 1c, a cooling time of 10 Gyr can not be obtained through a further increase of  $P_{ad}$  beyond 800 bar if  $L_{radio}(0)$  is not to drop below  $0.9 \times L_{cosmo}$ . The colder the interior, the lower  $T_{int}$  as predicted by our model atmosphere grid, and hence the intrinsic energy then can be transported through the radiative atmosphere. Enhancing  $P_{ad}(t_0)$  from 300 to 800 bar lowers  $T_{int}$  from 42.7 to 31.8 K (Table 1). For even colder interiors, the atmosphere is no longer capable of radiating away the heat generated by radioactive decay, which would contradict the assumption of such a cold interior.

The cooling time increases with the mass loss rate (Fig. 1d). For stellar XUV radiation  $F_{XUV}/F_{bol} = 10^{-5}$ – $10^{-4}$  as typical for quiet M-stars (Scalo et al. 2007), this enhancement is small (see Fig. 1d) and we obtain essentially the same range of  $P_{ad}(t_0)$  and hence structure models. Of GJ 1214b's initial total mass (initial H/He envelope mass), only 0.0054–0.013% (0.41–0.74%) is lost if  $F_{XUV}/F_{bol} = 10^{-5}$ , and about 0.1% (6%) if  $F_{XUV}/F_{bol} = 10^{-4}$ . On the other hand, for a permanent, strong irradiation  $F_{XUV}/F_{bol} = 10^{-3}$  as observed for young, active M-Stars listed in the ROSAT catalogue, GJ 1214b would have lost 1.8% (53%). These numbers are in agreement with the rough estimates in §2.3. In the last case, existence of a thin H/He atmosphere to-date

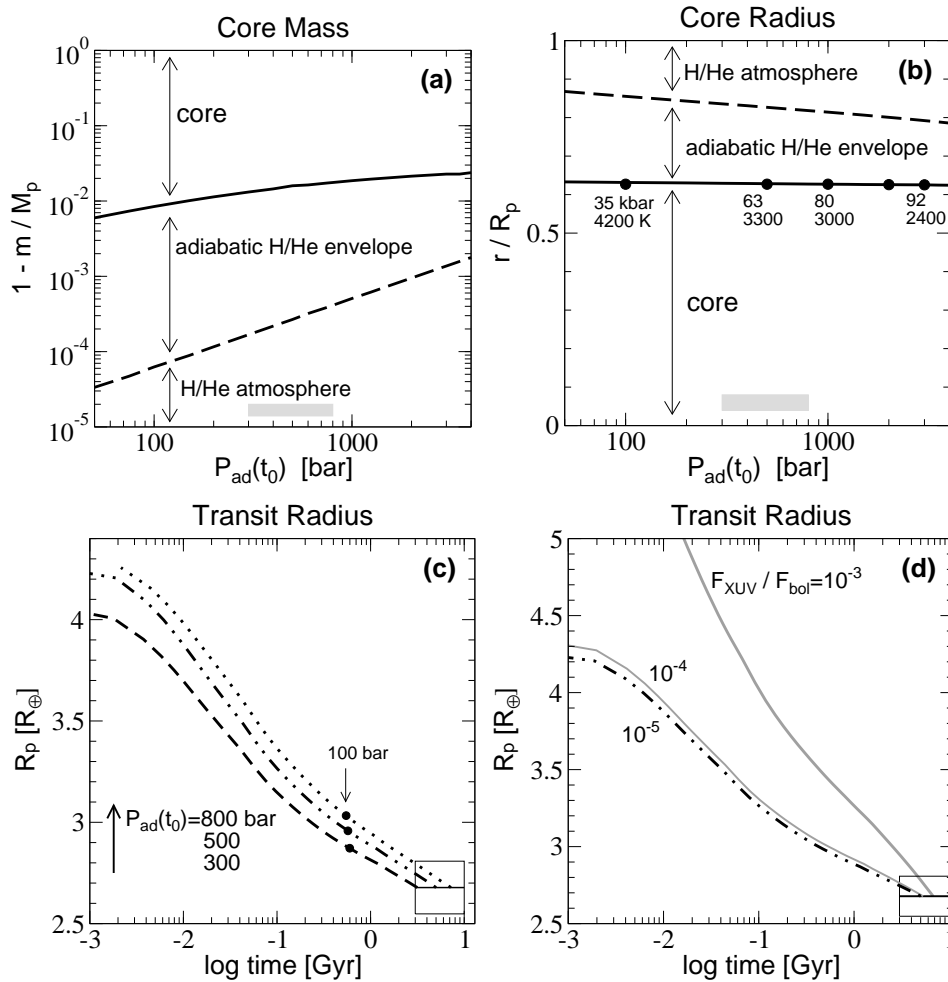


**Figure 1.** Cooling curves and internal structure of models with H/He envelope+rock core. All models are adjusted to have  $R_p(t_0) = 2.678R_\oplus$  by the choice of the core mass, and  $M_p(t_0) = 6.55M_\oplus$  at present time  $t_0$ . *Upper panels:* Mass (panel a) and radius (panel b) of the core (*solid line*) and where the atmosphere transitions into the adiabatic interior (*dashed*) of present time models with  $50 \leq P_{ad}(t_0) \leq 4000$  bar. Numbers are pressure in kbar and temperature in K at the envelope-core boundary for selected models. Single interior models run vertically. The *gray shaded areas* are a guide to the eye for the allowed  $P_{ad}(t_0)$  range that is consistent with the thermal evolution. *Lower panels:* Evolution of radius with time. *Panel c:* its dependence on  $P_{ad}(t_0)$ , *panel d:* on the insolation as parameterized by  $F_{XUV}/F_{bol}$ ; *dashed:* model Ia, *dotted:* model Ib (see Table 1), *dot-dot-dashed:* an intermediate one with  $P_{ad}(t_0) = 500$  bar. These cooling curves are for a specific heat of the core material  $c_v = 1.0$  J/gK and an insolation  $F_{XUV}/F_{bol} = 10^{-5}$  (*black*),  $10^{-4}$  (*thin solid gray*), and  $10^{-3}$  (*thick solid gray*). *Circles* in panel c indicate the profiles during evolution when  $P_{ad}(t) = 100$  bar. The *boxes* indicate the observational error bars of radius (vertical extension) and stellar age (horizontal extension).

becomes less likely since it begins to require fine-tuning of the initially accreted H/He envelope mass. We have found cooling tracks with an age of 10 Gyrs or more only if  $P \geq 800$  bar and the mass loss rate is high, or  $L_{radio}(t) \ll L_{cosmo}$ , which we do not favor.

Models with  $300 \leq P_{ad} \leq 800$  bar as constrained by our evolution calculations have  $M_{core} = 6.434 - 6.464M_\oplus$  and  $k_2 = 0.0170 - 0.0183$  implying a high degree of central condensation. The presence of an iron core could even enhance the central condensation. Therefore, although the H/He layer is low in mass, it significantly strengthens the property of central condensation compared to a closer to zero-mass atmosphere planetary object such as the Earth, the theoretical  $k_2$  value of which is  $\sim 0.3$  (Zhang 1991).

Class I models are closest to giant planets that formed within the snowline of the disk and did not have enough time and/or material in their surrounding to accrete a massive H/He envelope. Class I structure models can best be compared to ‘case I’ models by Rogers & Seager

(2010), where the difference in composition assumptions can be reduced to the core (undifferentiated rock core versus differentiated iron-silicate-water-ice core in their models), and a slightly different envelope He abundance of respectively 0.27 and 0.28.

Our obtained H/He mass fraction range, 1.3–1.8%, is due to the uncertainty in  $T_{int}$ . This range is much smaller than theirs ( $9 \times 10^{-3} - 6.8\%$ ), which includes uncertainties from the  $1\sigma$  errors of  $M_p$  and  $R_p$  contributing an uncertainty of 0.4–1.6%, from their  $T_{int}$  values used contributing up to 1.5%, and from the uncertainty in core composition (pure iron, iron-silicates-water, or pure water). Since iron is included in our rock EOS, we consider  $(1.8\% + 1.6\%) = 3.4\%$  a reliable upper limit of the H/He mass fraction if observations reveal a low-mean molecular weight atmosphere. Recent observations of GJ1214b’s atmosphere in the 0.78 to 1  $\mu\text{m}$  wavelengths range with the VLT facility’s UT1 telescope suggest a mean molecular weight of 5 g/mol or more and thus disfavor a H/He-dominated atmosphere (Bean et al. 2010). On the other

hand, the presence of clouds or hazes in such an atmosphere could mimic a short scaleheight, hence high mean molecular weight, and cannot be excluded by current observations and model atmospheres.

### 3.2. GJ 1214b as a water planet with a rock core

The derived core mass of water envelope+rock core models responds much more strongly to a change of the onset of the adiabatic part of the envelope than models with H/He envelope. At  $P_{ad}(t_0) \approx 400$  bar, the core mass reaches zero: a pure water planet (Fig. 2a). Deeper isothermal regions would only be possible if some amount of the pure water planet would be replaced by lighter elements such as methane or ammonia. Warming up the deep envelope by an outward shifting of the onset of the adiabatic region below 50 bar is accompanied by a strong rise in core mass. A solar water:rock ratio of 2.5 occurs for  $P_{ad} = 5$  bar—when the deep interior is extremely hot. Smaller ratios would be possible only if the isothermal region is allowed to disappear. We next consider whether such models are consistent with the cooling time.

Because of the relatively small core mass fraction of class II models, varying the specific heat of the core has a negligible effect on the cooling time. For  $80 \leq P_{ad}(t_0) \leq 300$  bar the resulting cooling times are consistent with  $\tau_*$ , see Table 1 and Fig. 2c. Those models have  $M_{core} = 0.20 - 0.87 M_{\oplus}$ , and a water:rock ratio of 6.5–31. This is much higher than the solar ice to rock ratio  $(I:R)_{\odot} \sim 2.5$ , which would give a cooling time shorter than 3 Gyr.

In contrast to models Ia,b, models IIa,b are weakly centrally condensed as parametrized by their high  $k_2$  values of respectively 0.57 and 0.74.

Class II models are different from those by Fu et al. (2010) who consider cold water planets with ice or liquid ocean layers above silicate/iron cores. GJ 1214b is not that cold. Our models also differ from the water steam atmosphere models of CoRoT-7b by Valencia et al. (2010) who find water envelope + silicate/iron core models where water in present CoRoT-7b contributes at most 10% to the total mass and is in the vapor phase or supercritical molecular phase. They also differ from the water steam atmosphere models by Rogers & Seager (2010) who describe the deep interior by a water-ice equation of state, whereas according to the phase diagram (Fig. 3) (updated from French et al. 2009; Valencia et al. 2010), water would be in the plasma phase in GJ 1214b.

In our class II models, water transitions from the vapor phase to supercritical molecular water still in the atmosphere, becomes dissociated into an ionic fluid at about 4000 K and 0.2 Mbar, and finally fully dissociated and ionized for  $T \geq 5100$  K and  $P \geq 1$  Mbar (Fig. 2b) forming a plasma with electronic conductivity  $\geq 100 \Omega/\text{cm}^2$  (Redmer et al. 2011).

Under these circumstances, a planetary interior can be able to maintain a dynamo generating a dipolar magnetic field. In Uranus and Neptune, the magnetic field may be generated in a thin shell (Stanley & Bloxham 2006) of possibly ionic water (Nellis et al. 1988). This view of the cold ( $T_{\text{eff}} \approx 59$  K) outer planets Uranus and Neptune is supported by the Neptune adiabat in Fig. 3, while in GJ 1214b, since it is warmer, the fluid conductive envelope would extend down to the small core, somewhat akin to Jupiter, and therefore preferably lead to a dipolar field, according to the field geometry considerations

by Stanley & Bloxham (2006).

### 3.3. GJ 1214b as a H/He/H<sub>2</sub>O planet with a rock core

This structure type resembles the outer envelope of Uranus and Neptune if  $Z_1 < 0.4$ , or their inner envelope if  $Z_1 > 0.7$  according to three-layer Uranus and Neptune models of Fortney & Nettelmann (2010). A strong enrichment in metals of the outer H/He layer in Uranus and Neptune is necessary to match the gravity field data, and also some admixture of light elements in the deep interior.

In § 3.2 we have seen that water envelope+rock core models of GJ 1214b yield supersolar I:R ratios of more than 2.6×solar. Lowering this ratio can be achieved by replacing water with hydrogen and helium. The two limiting cases of this implementation are a structure where a H/He layer is on top of a water layer, or a homogeneous mixture of H/He and H<sub>2</sub>O. We find that in the first case, such differentiated three-layer models (H/He, water, rock) can not have  $1 \times (I:R)_{\odot}$  and be in agreement with  $\tau_*$ , the reason of which is the following. Class I and class II models require a radiative atmosphere down to 80 bar or more at present in order to meet  $\tau_*$ . If composed solely of H/He, the atmosphere extends over about  $0.4 R_{\oplus}$ . In order to match a remaining radius  $r(M_p) \approx 2.3 R_{\oplus}$ , the core mass fraction of the remaining water+core body is of the order of 20–50% (see Valencia et al. 2010, Fig. 8). We find  $I:R < 0.9$  and  $M_{core} = 3.5 - 4.2 M_{\oplus}$  for this case of differentiated models. Increasing  $P_{ad}$  increases the depth of the thin H/He atmosphere, thereby lowering the I:R ratio even more. Increasing the planet’s mean density within the  $1\sigma$  error bars of  $M_p$  and  $R_p$  allows for I:R up to at most  $0.56 \times (I:R)_{\odot}$ .

Consequently, the only way to obtain a solar I:R ratio is to limit the radius of the H/He atmosphere by enhancing its mean molecular weight (Miller-Ricci et al. 2009) through admixture of water. Here we consider the case of equal metallicity in the radiative atmosphere and in the adiabatic envelope (our class III models) as parametrized by the water mass fraction  $Z_1$ . Figure 4a shows the change of the I:R ratio of single models. The water to core mass ratio rises moderately up to  $Z_1 = 0.9$ , passes  $1 \times (I:R)_{\odot}$  at  $Z_1 = 0.95$ , and then rises rapidly up to the values found for class II models. This behavior depends very weakly on the choice of  $P_{ad}(t_0)$ .

For class III models, the resulting H/He mass fraction of the planet (see Fig. 4a) is about 2–3 times larger than in case of a H/He layer on top of a water layer. It reaches the maximum for  $Z_1 \approx 0.80$  (the core mass must not be too large, requiring a high metallicity, and also  $Z_1$  not too close to 1). We find a planetary H/He mass fraction  $\leq 5.9\%$  if  $P_{ad}(t_0) = 400$  bar as in Fig. 4a,b, and slowly rising with  $P_{ad}(t_0)$  up to 7% (colder envelopes reduce the core mass). However, a colder present time interior would take longer than 10 Gyrs to cool. For the cooling curve calculations we choose a metallicity  $Z_1 = 0.85$ , which gives a H/He mass fraction close to the maximum value but also a core mass below  $2/3 M_p$ , hence a real alternative to classes I and II. Figure 4c shows that the isothermal region of present GJ 1214b must end between 120 and 400 bar to give consistency with a cooling time of 3 to 10 Gyrs.

With  $Z_1 = 0.85$ ,  $T_{core} = 5730$  K, and  $P_{core} =$

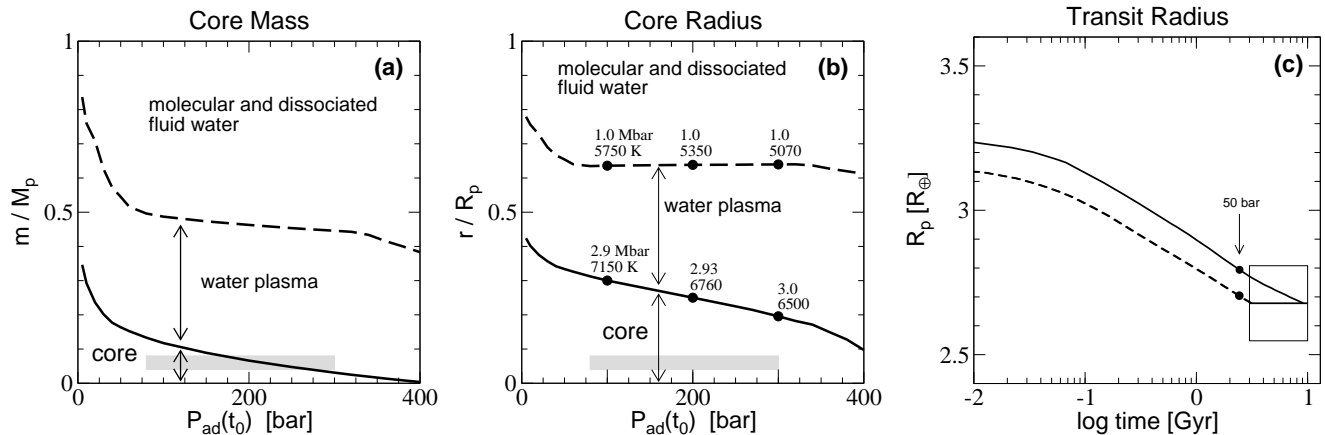


**Figure 2.** Cooling curves and internal structure of models with water envelope+rock core. All models are adjusted to have  $R_p(t_0) = 2.678R_\oplus$  by the choice of the core mass. *Left (panel a):* Core mass (solid line) and mass shell where water in the envelope enters the plasma phase (dashed line) of present time structure models for transition pressures  $5 \leq P_{ad}(t_0) \leq 400$  bar. Single interior models run vertically. The gray shaded areas are a guide to the eye for the allowed  $P_{ad}(t_0)$  range that is consistent with the thermal evolution (in panel c). *Middle (panel b):* Same as (a) but radius coordinate. Numbers at models highlighted by filled circles are pressure in Mbar and temperature in K. *Right (panel c):* Evolution of radius of structure models IIa (dashed) and IIb (solid), see Table 1. Circles indicate those profiles during evolution when  $P_{ad}(t_0) = 50$  bar.

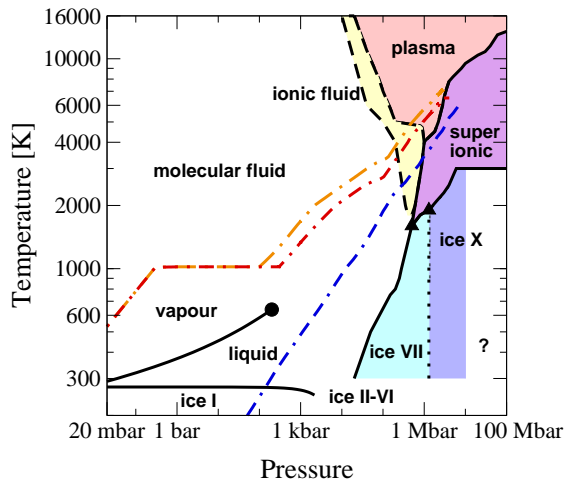


**Figure 3.** Water phase diagram for  $20 \text{ mbar} < P < 100 \text{ Mbar}$  and GJ 1214b water envelope+rock core models with  $P_{ad}(t_0) = 100$  bar (orange dashed-dot) and 300 bar (red dashed-dot). The Neptune profile (blue dashed-dot) is adopted from Redmer et al. (2011).

1.4 Mbar (Fig. 4b), model IIIb resembles the interior of Uranus and Neptune in composition and temperature (Fortney & Nettelmann 2010). Lower in total mass, the pressure does not rise up to 5–7 Mbar as in the outer solar system giant planets, so that water will not adopt the superionic phase according to the phase diagram of water, but remain in a fluid state in GJ 1214b (Fig. 3). This property bolsters our assumption of a homogeneous mixture of water with hydrogen and helium.

## 4. DISCUSSION

### 4.1. Structure assumptions

Our GJ 1214b interior models rely on a separation of the interior into a rock core and one homogeneous envelope of the same composition as in the visible atmosphere. In contrast, giant and terrestrial planets in the solar system are not successfully described by such a two-layer structure but require the assumption of various internal layer boundaries to be consistent with the atmospheric He abundance and the gravity field data (giant plan-

ets: see Gudkova & Zharkov 1999; Saumon & Guillot 2004; Nettelmann et al. 2008; Fortney & Nettelmann 2010), long-term spacecraft tracking data (Mars: see Konopliv et al. 2006), and with seismic data (Earth).

#### 4.1.1. class III: H/He phase separation?

For the giant planets, a layered structure is suggested in part because of a measured atmospheric depletion in He indicating H/He phase separation, and in part because of relatively low measured  $J_4/J_2$  ratios indicating an enhancement with metals in the deep interior. According to experimental and theoretical data on H/He demixing (see e.g. Lorenzen et al. 2009; Morales et al. 2009), immiscibility of He in H might also occur in our class III models close to the core-mantle boundary. Given the low interior temperatures (relative to Saturn) this could very strongly deplete most of the envelope in helium (Fortney & Hubbard 2004). While accurate measurements of the atmospheric He abundances are extraordinarily difficult to perform without the use of entry probes even in case of solar giant planets, this effect can affect the current depth of the isothermal region (120–400 bar) that we have derived from the cooling time calculations. This would be a completely different pathway towards a helium-depleted hydrogen atmosphere than the outgassing scenario discussed in Rogers & Seager (2010). On the other hand if  $Z_1 \ll 0.85$ , then the envelope does not become massive and dense enough for He sedimentation to occur.

#### 4.1.2. class II: Incomplete Differentiation?

Our class II models require a process that causes a downward sedimentation of rocks in order to separate out a water layer, as in Ganymede (Kirk & Stevenson 1987). Up to now, there is no experimental evidence that water and silicates or iron become immiscible under high pressure, and the timescale for gravitational settling before the onset of convection, terminating gravitational settling, is essentially unknown for Ganymede (Kimura et al. 2009). Since the larger primordial heat deposited in the  $\sim 260$  times more massive GJ 1214b



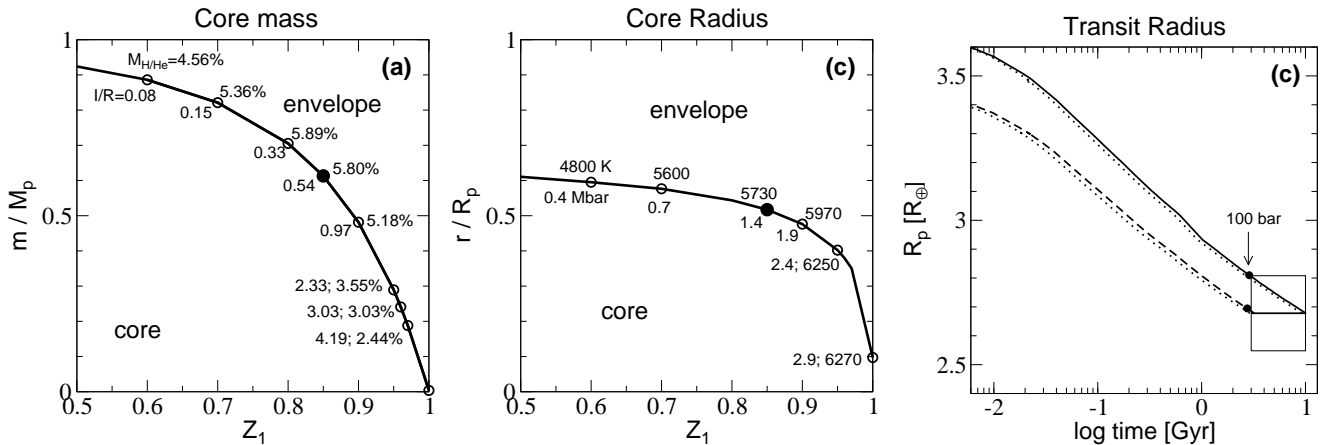


**Figure 4.** Cooling curves and internal structure of H/He/H<sub>2</sub>O envelope+rock core models with various envelope metallicities. *Left:* The dependence of the core mass (in  $M_p$ ) on the envelope metallicity  $Z_1$  of present time structure models with  $P_{ad}(t_0) = 400$  bar. Numbers at selected models are the I/R ratio (*first number*) and the entire planet’s H/He mass fraction in percent. Model IIIb is highlighted (*filled circle*). *Middle:* Core radius in  $R_p$ . Numbers are pressure in Mbar and temperature in K at the envelope-core boundary for the same models as in the left panel. *Right:* Evolution of radius with time for models IIIa (*dashed*) and IIIb (*solid*), see Table 1, using specific heat of the core material  $c_v = 1.0$ , or  $0.5 \text{ J/gK}$  (*dotted*). Circles in panel c indicate those profiles during evolution when  $P_{ad}(t) = 100$  bar.

might have caused a rapid onset of convection, a water+rock interior of GJ 1214b is possibly not fully differentiated. Internal layer boundaries dividing regions with different water to rock ratios can not be excluded, and the core rather be an ice-rock mixture as suggested for Callisto (Nagel et al. 2004) than pure rocks. On the other hand, more detailed envelope models of GJ 1214b would be underdetermined by current observational parameters.

#### 4.1.3. class I: Choked off giant planet formation?

The core mass of our class I models is within the range of rock core masses currently proposed for Jupiter (Fortney & Nettelmann 2010). With an initial H/He atmosphere of only 1–2%  $M_p$ , GJ 1214b appears to be a giant planet whose envelope mass accretion was choked off during formation. It is of general interest for more super-Earth planets to be detected to see whether this is a common outcome of planet formation.

### 4.2. Composition

From interior and atmosphere models that are consistent with the observationally derived parameters  $T_{\text{eq}}$ ,  $M_p$ , and  $R_p$  after 3–10 Gyrs of cooling, the most certain conclusion we can draw about the composition of GJ 1214b is a metallicity of 94–100%. The lower limit can further shrink somewhat if the planet in reality is dry, and the mass fraction of water in our class III models then resembles a mixture of H/He and rocks. In contrast, the mass fractions of water, used as a proxy for the ices H<sub>2</sub>O, CH<sub>4</sub>, NH<sub>3</sub>, and H<sub>2</sub>S, is essentially unconstrained (0–97%) as is the mass fraction of rocks (3–99%).

Two further observables we can hope to attain in the near future are the Love number  $k_2$  from transit timing variations or from the shape of the transit light curves (Ragozzine & Wolf 2009), and second the mean molecular weight in the atmosphere from transmission spectroscopy, in particular from the wavelength dependence of star light absorption in the planetary atmosphere during transit (Miller-Ricci & Fortney 2010).

#### 4.2.1. Love number $k_2$

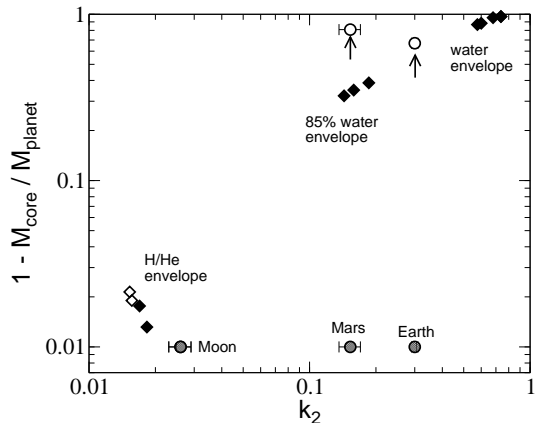


**Figure 5.** Collection of  $\{M_{\text{core}}, k_2\}$  pairs obtained for class I–III models of GJ 1214b (*diamonds*), that meet the age constraint (*filled*) or not (*open*); and measured  $k_2$  values with error bars of Moon, Mars, and Earth (M M E) (*circles*). According to the definition of  $M_{\text{core}}$  used for GJ 1214b, M M E would have  $M_{\text{core}} > 0.999999M_p$ , which we placed at  $0.99M_p$ . Considering alternatively  $M_{\text{core}}$  as the iron core of these objects shifts the *filled circles* to the *open circles*. This figure demonstrates degeneracy of  $k_2$  in two-layer models with thin atmospheres.

The  $k_2$  values of models from our classes I–III differ greatly from each other and thus we consider  $k_2$  a useful quantity to discriminate between atmospheres of different mean molecular weight. The trend of decreasing  $k_2$  value with increasing core mass that is known for two-layer models of Jupiter-mass giant planets with a core and one envelope (Batygin et al. 2009b), or for  $n=1$  polytropic planets in general (Kramm et al. 2011), is confirmed by our two-layer models of GJ 1214b. An illustration of the  $k_2(M_{\text{core}})$  behavior is shown in Fig. 5, which contains the same data as Table 1 and also some intermediate points as well as two solutions of the H/He envelope models with respectively  $P_{ad}(t_0) = 1$  and 2 kbar, which are too cold as explained in § 3.1.

However, when the H/He atmosphere becomes thin and its mass low enough ( $< 2\%$ ), this planet begins to more closely resemble a relatively homogeneous rock body than a core+envelope planet, and  $k_2$  rises again. This degeneracy of  $k_2$  that is otherwise well-known for

multi-layer models is –at first glance– a surprising finding in *two-layer* super-Earth models. As Fig. 5 suggests, pure H atmosphere models of GJ1214b (Rogers & Seager 2010) would approach the  $k_2$  values of solar system bodies such as the Moon, i.e. *higher* than that of H/He atmospheres.

Moon, Mars, and Earth can be considered as remnant protoplanetary cores ( $M_{core} = M_p$ ) that did not accumulate sufficient mass to accrete a significant envelope. On the other hand, because measured  $k_2$  values of Earth (see Ray et al. 2001), Mars (Yoder et al. 2003; Konopliv et al. 2006), and Moon (Zhang 1992) cannot be explained by a homogeneous rock interior but require the assumption of a dense, iron-rich core (e.g. Zharkov et al. 2009), they can also be considered as objects with small (iron) core and large (silicate) mantle ( $M_{core} \ll M_p$ ). This places Mars and Earth close to our GJ 1214b models with H/He/Z envelope in the  $k_2 - M_{core}$  diagram, implying that  $k_2$  is a degenerate quantity with respect to composition, too. Separation into layers of different composition owing to phase differentiation and phase transitions in rocks (Valencia et al. 2007) has likely also occurred in GJ 1214b. Such an advanced treatment of a core would enhance the level of central condensation, and result in even lower minimum  $k_2$  values below 0.017. The same trend is expected for inclusion of solid-body effects, which will be important for colder super-Earth planets and those with less extended, less massive atmosphere. Theoretical  $k_2$  values for the terrestrial objects are in good agreement with the observations when making the simplifying assumption of an elastic interior (Zhang 1992; Yoder et al. 2003) (in which case the shear modulus becomes frequency-independent, i.e.  $k_2$  a static Love number), while their observed moments of inertia are close to 0.4 indicating a nearly homogeneous interior, the theoretical Love number  $k_2$  of which would approach 1.5 if the body were fluid and compressible.

#### 4.2.2. Mean molecular weight

Class III models with  $1\times$ solar I:R ratio are not excluded by our thermal evolution calculations. Those models require  $Z_1 = 0.95$ , corresponding to a mean molecular weight  $\mu = 13.4 \text{ g mol}^{-1}$  and  $440\times$ solar O:H particle number ratio (assuming a solar O:H of  $0.85 \times 10^{-3}$  according to Anders & Grevesse 1989). However, we do not consider such models a realistic description of GJ 1214b. For rapid translations between metallicity and atmospheric  $\mu$  values from transmission spectroscopy observations, we present the simple relations between  $\mu$ , O:H, and  $Z_1$  in Fig. 6.

In particular, our class III models with  $Z_1 = 0.85$  have  $\mu = 8.9 \text{ g mol}^{-1}$ , a  $270\times$  solar atmospheric O:H ratio, 0.2 times solar bulk I:R ratio, and  $\approx 5.8\%$  of  $M_p$  is H/He. For  $Z_1 < 0.55$ , our class III models become severely rock-dominated with  $M_{core} > 0.9M_p$ ,  $\mu < 4.4 \text{ g mol}^{-1}$  and O:H  $< 92\times$ solar. A  $50\times$ solar O:H ratio as of our model atmosphere grid applied to the thermal evolution calculations (see § 2.1) implies  $Z_1 = 0.38$ . For  $\mu = 5 \text{ g mol}^{-1}$  as suggested from the first transmission spectrum observations by Bean et al. (2010), Fig. 6 gives  $Z_1 = 0.7$  and according to Fig. 4, GJ1214b could be mostly rocky with an I:R ratio of 0.15, where the H/He/H<sub>2</sub>O atmosphere contributes  $\sim 18\%$  to the planet’s mass and 40% to its radius.

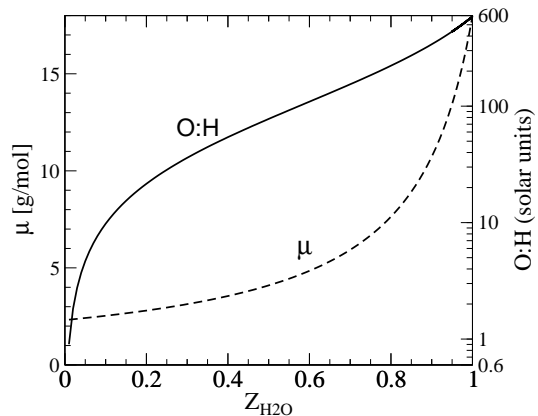


**Figure 6.** Mean molecular weight (*dashed*) and O:H ratio (*solid*) of H/He/H<sub>2</sub>O mixtures with water mass fraction  $Z$  and  $Y=0.27$ .

## 5. CONCLUSIONS

Our results for the composition of the super-Earth mass planet GJ 1214b confirm that it has a gaseous atmosphere atop a fluid envelope. We find a minimal total H/He mass fraction of 1.3% for pure H/He envelopes, which can rise to 5–6% if the envelope contains 60–90% H<sub>2</sub>O in mass, and even further if also silicates and iron are mixed into the envelope.

Water in GJ 1214b does not solidify within 10 Gyrs of cooling, and it not a liquid as is found on Earth’s surface, but becomes a plasma if its abundance is high ( $Z_1 > 0.8$ ). This leads to a large water mass ( $> 1/3M_p$ ), where the deep internal matter is warm ( $T > 5500 \text{ K}$ ) and dense ( $P > 1 \text{ Mbar}$ ).

The intrinsic heat loss of GJ 1214b after 3–10 Gyr of cooling corresponds to  $T_{int} = 32 - 52 \text{ K}$ , where the lower bound depends on assumptions about the heat production by radioactive elements and slightly on mass loss. By our self-consistent mass-loss calculations we conclude that GJ 1214b is a genuine super-Earth that has lost an insignificant amount of its initial mass, unlike CoRoT-7b.

Nevertheless, some of our computed models may fall into the realm of the unlikely. These include class I models that have lost more than 50% of their initial H/He envelope (i.e.  $2\%M_p$  lost) due to extraordinary XUV irradiation and thus require fine-tuning of their initial H/He mass fraction. Moreover, extremely low-mass H/He atmospheres in general might be an unlikely outcome of planet formation. The unlikelihood of forming a massive planet with an extreme ice-to-rock ratio of more than 6 casts our class II (“water world”) models in doubt. We instead favor what is thought to be the most Uranus- and Neptune-like planet models, class III. It includes envelopes with  $\sim 85\%$  water by mass mixed into H and He atop a rock core with about  $0.2\times$  solar bulk ice:rock ratio. These models have higher H/He masses (5.8% of the planet mass) than class I models with pure H/He atmospheres, lessening worries about the survival of a H/He envelope in the face of mass loss. A general outcome of these models is  $T_{int} = 42 \pm 6 \text{ K}$ , while the conditions at the core-mantle boundary are  $P \approx 1 \text{ Mbar}$  and  $T \approx 5700 \text{ K}$ . The atmosphere can be strongly depleted in helium due to H/He phase separation deeper inside the planet (if  $Z_1 \sim 0.85$ ) or not be depleted in He if  $Z_1$  is much smaller than this.

Calculated Love numbers of water envelope models

that are consistent with the observables  $M_p$ ,  $R_p$ ,  $T_{\text{eq}}$ , and the age, are in the range  $k_2 = 0.58\text{--}0.74$ , whereas pure H/He envelope models have  $k_2 \sim 0.018$ , and our favorite models  $k_2 \sim 0.15$ . An observational determination of  $k_2$  and the atmospheric mean molecular weight is crucial for determining the envelope metallicity and the core mass of this and other planets that are located along the  $M - R$  relation of water planets. However, ambiguities in composition are an inherent property of such planets.

We thank E. Kempton (formerly Miller-Ricci) for discussion and the delivery of her solar composition and water model atmospheres, T. Guillot and D. Valencia for valuable comments on the radioactive luminosity of rock material, and F. Sohl for helpful discussions on dynamic Love numbers. This work was supported by the NASA, under grants NNX08AU31G and NNX09AC22G, and DFG under grants RE 882/11 and RE 882/12.

## REFERENCES

- Alfè, D., Price, G. D., & Gillan, M. J. 2001, *Phys. Rev. B*, 64, 045123
- Anders, E., & Grevesse, N. 1989, *GeCoA*, 53, 197
- Baraffe, I., Chabrier, G., & Barman, T. 2008, *A&A*, 482, 315
- Baraffe, I., Chabrier, G., Barman, T. S., Allard, F., & Hauschildt, P. 2003, *A&A*, 402, 701
- Batygin, K., Bodenheimer, P., & Laughlin, G. 2009b, *ApJ*, 704, L49
- Bean, J. L., Miller-Ricci Kempton, E., & Homeier, D. 2010, *Nature*, 468, 669
- Charbonneau, D., Zachory, B. K., Irwin, J., et al. 2009, *Nature*, 462, 891
- Erkaev, N. V., Kulikov, Y. N., Lammer, H., Selsis, F., D., L., Jaritz, G. F., & Biernat, H. K. 2007, *A&A*, 472, 329
- Feistel, R., & Wager, W. 2006, *Phys. Chem. Ref. Data*, 35, 1021
- Fortney, J. J., & Hubbard, W. B. 2004, *ApJ*, 608, 1039
- Fortney, J. J., Ikoma, M., Nettelmann, N., Guillot, T., & Marley, M. S. 2010b, *ApJ*, 729, 32
- Fortney, J. J., Marley, M. S., & Barnes, J. W. 2007, *ApJ*, 659, 1661
- Fortney, J. J., Marley, M. S., Hubickyj, O., Bodenheimer, P., & Lissauer, J. J. 2005, *AN*, 326, 925
- Fortney, J. J., & Nettelmann, N. 2010, in *Springer Space Science Reviews*, Vol. 157, Planetary Magnetism, ed. U. Christensen, A. Balogh, D. Breuer, & K.-H. Glaßmeier, 423–447
- Fortney, J. J., Sudarsky, D., Hubeny, I., Cooper, C. S., Hubbard, W. B., Burrows, A., & Lunine, J. I. 2003, *ApJ*, 589, 615
- Freedman, R. S., Marley, M. S., & Lodders, K. 2008, *ApJS*, 174, 504
- French, M., Mattsson, T. R., Nettelmann, N., & Redmer, R. 2009, *Phys. Rev. B*, 79, 954107
- Fu, R., O’Connell, R., & Sasselov, D. D. 2010, *ApJ*, 708, 1326
- Gudkova, T. V., & Zharkov, V. N. 1999, *Planet. Space Sci*, 47, 120
- Guillot, T. 1999, *Science*, 296, 72
- Guillot, T., Burrows, A., Hubbard, W. B., Lunine, J. I., & Saumon, D. 2006, *ApJ*, 459, L35
- Guillot, T., Chabrier, G., Gautier, D., & Morel, P. 1995, *ApJ*, 450, 463
- Guillot, T., & Gautier, D. 2009, arXiv:0912.2019v1
- Hubbard, W. 1977, *Icarus*, 30, 305
- Hubbard, W. B. 1984, *Planetary Interiors* (Van Nostrand Reinhold Company Inc.)
- Hubbard, W. B., & Marley, M. S. 1989, *Icarus*, 78, 102
- Hubbard, W. B., Podolak, M., & Stevenson, D. J. 1995, in *Neptune and Triton*, ed. Cruikshank (University of Arizona, Tucson), 109–138
- Jackson, B., Miller, N., Barnes, R., Raymond, S. N., Fortney, J. J., & Greenberg, R. 2010, *MNRAS*, 407, 910
- Kerley, G. 2004, *An equation of state of Helium*, Tech. rep., KTS04-2
- Kimura, J., Nakagawa, T., & Kurita, K. 2009, *Icarus*, 202, 216
- Kirk, R. L., & Stevenson, D. J. 1987, *Icarus*, 69, 91
- Konopliv, A. S., Yoder, C. F., Standish, E. M., Yuan, D.-N., & Sjogren, William, L. 2006, *Icarus*, 182, 23
- Kramm, U., Nettelmann, N., Redmer, R., & Stevenson, D. S. 2011, *A&A*, 528, A18
- Lammer, H., Selsis, F., Ribas, I., Guinan, E. F., Bauer, S. J., & Weiss, W. W. 2003, *ApJ*, 598, L121
- Léger, A., Rouan, D., Schneider, R., et al. 2009, *A&A*, 506, L287
- Lorenzen, W., Holst, B., & Redmer, R. 2009, *Phys. Rev. Lett.*, 102, 5701
- Lyon, S., & Johnson, J. D. e. 1992, *SESAME: Los Alamos National Laboratory Equation of State Database*, Tech. rep., LANL report no. LA-UR-92-3407
- Mardling, R. A. 2010, *MNRAS*, 410, 1048
- McDonough, W. F., & Sun, S.-S. 1995, *Chem. Geology*, 120, 223
- Miller, N., Fortney, J. J., & Jackson, B. 2009, *ApJ*, 702, 1413
- Miller-Ricci, E., & Fortney, J. J. 2010, *ApJ*, 716, L74
- Miller-Ricci, E., Seager, S., & Sasselov, D. 2009, *ApJ*, 690, 1056
- Morales, M. A., Schwegler, E., Ceperly, D., Pierleoni, C., Hamel, S., & Caspersen, K. 2009, *PNAS*, 106, 1324
- Murray-Clay, R., Chiang, E. I., & Murray, N. 2009, *ApJ*, 693, 23
- Nagel, K., Breuer, D., & Spohn, T. 2004, *Icarus*, 169, 402
- Nellis, W. J., Hamilton, D. C., Holmes, N. C., Radosky, H. B., Ree, F. H., Mitchell, A. C., & Nicol, M. 1988, *Science*, 240, 779
- Nettelmann, N., Holst, B., Kietzmann, A., French, M., Redmer, R., & Blaschke, D. 2008, *ApJ*, 683, 1217
- Nettelmann, N., Kramm, U., Redmer, R., & Neuhäuser, R. 2010, *A&A*, 523, A26
- Ragozzine, D., & Wolf, A. S. 2009, *ApJ*, 698, 1778
- Ray, R. D., Eanes, R. J., & Lemoine, F. G. 2001, *Geophys. J. Int.*, 144, 471
- Redmer, R., French, M., Nettelmann, N., & Mattsson, T. R. 2011, *Icarus*, 211, 798
- Rogers, L. A., & Seager, S. 2010, *ApJ*, 716, 1208
- Sada, P. V., et al. 2010, *ApJ*, 720, L215
- Saumon, D., Chabrier, G., & van Horn, H. M. 1995, *ApJ*, 99, 713
- Saumon, D., & Guillot, T. 2004, *ApJ*, 609, 1170
- Scalo, J., et al. 2007, *Astrobiology*, 7, 85
- Seager, S., Kuchner, M., Hier-Majumder, C. A., & Militzer, B. 2007, *ApJ*, 669, 1279
- Stanley, S., & Bloxham, J. 2006, *Icarus*, 184, 556
- Valencia, D., Ikoma, M., Guillot, T., & Nettelmann, N. 2010, *A&A*, 516, A20
- Valencia, D., Sasselov, D. D., & O’Connell, R. J. 2007, *ApJ*, 656, 545
- Vidal-Madjar, A., Lecavalier des Etangs, A., Desert, J.-M., Ballester, G. E., Ferlet, R., Hebrard, G., & Mayor, M. 2003, *Nature*, 422, 143
- Wagner, W., & Pruß, A. 2002, *J. Phys. Chem. Ref. Data*, 31, 387
- Yelle, R. V. 2004, *Icarus*, 170, 167
- Yoder, C. F., Konopliv, A. S., Yuan, D. N., Standish, E. M., & Folkner, W. M. 2003, *Science*, 300, 299
- Zhang, C. Z. 1991, *Earth, Moon, and Planets*, 54, 129
- . 1992, *Earth, Moon, and Planets*, 56, 193
- Zharkov, V. N., Gudkova, T. V., & Molodensky, S. M. 2009, *PEPI*, 172, 324
- Zharkov, V. N., & Trubitsyn, V. P. 1978, *Physics of Planetary Interiors* (Tucson: Parchart)